Published in final edited form as:
J Magn Reson Imaging. 2011 April ; 33(4): 873–881. doi:10.1002/jmri.22514.

T_1 Independent, T_2^* Corrected Chemical Shift Based Fat–Water Separation With Multi-peak Fat Spectral Modeling Is an Accurate and Precise Measure of Hepatic Steatosis

Catherine D.G. Hines, PhD[1], **Alex Frydrychowicz, MD**[1,2], **Gavin Hamilton, PhD**[3], **Dana L. Tudorascu, PhD**[4], **Karl K. Vigen, PhD**[1], **Huanzhou Yu, PhD**[5], **Charles A. McKenzie, PhD**[6], **Claude B. Sirlin, MD**[3], **Jean H. Brittain, PhD**[7], and **Scott B. Reeder, MD, PhD**[1,8,*]

[1]Liver Imaging Research Program, Department of Radiology, University of Wisconsin, Madison, Wisconsin, USA

[2]Department of Diagnostic Radiology and Medical Physics, University Hospital Freiburg, Freiburg, Germany

[3]Liver Imaging Group, Department of Radiology, University of California, San Diego, California, USA

[4]Waisman Laboratory for Brain Imaging and Behavior, University of Wisconsin, Madison, Wisconsin, USA

[5]Applied Science Laboratory, GE Healthcare, Menlo Park, California, USA

[6]Department of Medical Biophysics, University of Western Ontario, London, Ontario, Canada

[7]Applied Science Laboratory, GE Healthcare, Madison, Wisconsin, USA

[8]Departments of Medical Physics, Biomedical Engineering, and Medicine, University of Wisconsin, Madison, Wisconsin, USA

Abstract

Purpose—To determine the precision and accuracy of hepatic fat-fraction measured with a chemical shift-based MRI fat-water separation method, using single-voxel MR spectroscopy (MRS) as a reference standard.

Materials and Methods—In 42 patients, two repeated measurements were made using a T_1-independent, T_2^*-corrected chemical shift-based fat-water separation method with multi-peak spectral modeling of fat, and T_2-corrected single voxel MR spectroscopy. Precision was assessed through calculation of Bland-Altman plots and concordance correlation intervals. Accuracy was assessed through linear regression between MRI and MRS. Sensitivity and specificity of MRI fat-fractions for diagnosis of steatosis using MRS as a reference standard were also calculated.

Results—Statistical analysis demonstrated excellent precision of MRI and MRS fat-fractions, indicated by 95% confidence intervals (units of absolute percent) of [−2.66%,2.64%] for single MRI ROI measurements, [−0.81%,0.80%] for averaged MRI ROI, and [−2.70%,2.87%] for single-voxel MRS. Linear regression between MRI and MRS indicated that the MRI method is highly accurate. Sensitivity and specificity for detection of steatosis using averaged MRI ROI

*Address reprint requests to: S.B.R., Department of Radiology, E1/374 CSC, University of Wisconsin, 600 Highland Avenue, Madison, WI 53792-3252. sreeder@wisc.edu.

were 100% and 94%, respectively. The relationship between hepatic fat-fraction and body mass index was examined.

Conclusion—Fat-fraction measured with T_1-independent T_2^*-corrected MRI and multi-peak spectral modeling of fat is a highly precise and accurate method of quantifying hepatic steatosis.

Keywords

fat quantification; MRI; hepatic steatosis; nonalcoholic fatty liver disease; MR spectroscopy

---

Nonalcoholic Fatty Liver disease (NAFLD) is the most common cause of chronic liver disease in Western societies with an increasing prevalence that parallels current epidemics of obesity and diabetes (1,2). NAFLD is considered by many to be the hepatic manifestation of the metabolic syndrome, a constellation of diseases including adult-onset diabetes (type II), hyperlipidemia, and obesity (3,4). Individuals with NAFLD can progress to a more aggressive form of NAFLD known as nonalcoholic steatohepatitis (NASH), which is characterized by inflammation, ballooning degeneration and fibrosis, in addition to steatosis (5,6). Many patients with steatohepatitis progress to end-stage fibrosis (cirrhosis), which predisposes patients to hepatocellular carcinoma (HCC) and liver failure (7,8).

Intracellular accumulation of triglycerides and fatty acids (steatosis) is the earliest and hallmark histological feature of NAFLD. Definitive diagnosis of NAFLD and grading of steatosis requires biopsy, which is regarded as the clinical gold standard test and is the current standard of care. Biopsy, however, is limited by cost, high sampling variability (9), and other significant risks that limit its utility for repeated evaluation of liver disease. For these reasons, a noninvasive, cost-effective, and quantitative alternative to biopsy is needed for accurate quantification of hepatic steatosis.

MRI is highly sensitive to the presence of fat due to differences in chemical shift between water and fat. MR spectroscopy (MRS) is considered by many to be the noninvasive reference standard for quantification of hepatic fat content (10,11). MRS has both higher sensitivity and specificity for hepatic fat quantification compared with ultrasound and computed tomography (12), indicating that an MR-based technique would be advantageous for hepatic fat quantification. However, like biopsy, MRS is prone to sampling error due to the heterogeneity of steatosis because typically only a single voxel is used to assess the entire liver. Alternatively, chemical shift based water–fat separation methods have demonstrated accurate quantification of hepatic steatosis by several groups (11,13–17).

Several confounding factors have been identified that corrupt the ability of MRI to accurately quantify fat using fat–water separation techniques (18). These factors must be addressed before the measured fat-fraction accurately reflects the underlying concentration of triglycerides. Specific confounding factors include T_1 bias (13, 19–21), noise bias (19), the complex NMR spectrum of fat (13,14,22), T_2^* decay (13,23), and phase errors caused by eddy currents (24). To perform the correction for eddy currents, a complex image-based fat-water separation including spectral modeling and T_2^* correction is performed first. Then, a second fit to a magnitude signal model is performed, using the complex estimates of water, fat and T_2^* as the starting conditions. This provides estimates of water and fat that are free from the effects of phase shifts from eddy currents. After correction for all confounding factors, the measured fat-fraction is equivalent to the proton density fat-fraction (PDFF). PDFF is an inherent property of the tissue, and is platform and protocol independent, making it a potentially useful biomarker of liver fat content.

A recently described complex chemical shift-based fat-water separation method, based on IDEAL (Iterative Decomposition of water and fat with Echo Asymmetry and Least squares estimation) has been described for fat quantification in the liver (14,19,22,23,25). Using a low flip angle to minimize T_1 bias (19), magnitude discrimination to minimize noise bias (19), T_2^* correction (22,23), multi-peak fat spectral modeling (14,22) including six spectral peaks of fat, and eddy current correction (24), accurate quantification has been validated in phantom experiments (26), animal experiments (17) and more recently in in vivo studies (25), over a wide range of fat-fractions (17,26). These studies collectively provide validation on the accuracy of this method.

However, rigorous validation of a biomarker also requires an understanding of the precision (repeatability) of a method to assess longitudinal changes in the biomarker. Therefore the primary purpose of this work is to determine the precision of clinical MRI hepatic fat quantification when correction for all known confounding factors has been performed. A secondary purpose is to reproduce accuracy measurements reported in previous validation studies (25), using MRS as the reference standard for hepatic fat-fraction.

Patients and Methods

Patients

After obtaining IRB approval and informed consent, 42 patients (22 male, 20 female) referred to the Department of Radiology for abdominal MRI were recruited for this study, irrespective of diagnosis, between September 16, 2009 and August 20, 2010. Mean age for all patients was 51.0 ± 13.1 years (range, 23–80 years). Thirty-five of these patients had height and weight recorded in the medical record; these patients had a mean weight of 82.0 ± 25.8 kg (range, 50.3–207 kg), and a mean body mass index (BMI) of 24.6 ± 5.5 kg/m^2 (range, 19.1–45.3 kg/m^2). All patients over the age of 18 were eligible for this study, and no patients were excluded, unless they declined to consent to the study.

Imaging Protocol

Imaging was performed on three 1.5 Tesla (T) clinical scanners (Signa HDx, GE Healthcare, Waukesha, WI) using an eight-channel phased array cardiac coil or eight-channel body phased array coil.

For each patient, two repeated measurements of a quantitative chemical shift-based water–fat separation MRI method and a single voxel MRS were made to assess repeatability (precision) of both techniques. Between each measurement (“Time 1” and “Time 2”), the patient was removed from the magnet, and the anterior coil elements only removed. The patient was instructed to sit up and then lie down, after which the anterior coil was repositioned and the patient placed back into the magnet without disturbing the posterior coil. New landmarks and new localizers were acquired, and all prescanning was repeated, followed by re-prescription of the MRI and MRS sequences to simulate a new, independent exam.

For volumetric MRI fat-fraction imaging, an investigational version of the three-dimensional spoiled gradient echo (SPGR) IDEAL sequence was used (27). Using fly-back readouts, a total of six echoes were acquired per TR, and a 2D parallel imaging acceleration method (ARC) (28,29), which had an effective net acceleration of 2.2, was used to reduce the total imaging time to 21 s. Imaging parameters for the MRI sequence were: first TE =1.3 ms, echo spacing = 2.0 ms, TR = 13.7 ms, BW = ± 125 kHz, FOV = 35 × 35 cm, slice =10 mm, 256 × 128 matrix, flip = 5° to reduce T_1 bias (19), and 24 slices in the superior/inferior

direction. Thus, complete liver coverage was acquired in one breath-hold, with true spatial resolution of 1.4 – 2.7 – 10 mm.

Single voxel breath-held MRS data were acquired to provide a reference fat-fraction. Spectra were acquired using an investigational version of STEAM (Stimulated Echo Acquisition Mode) without water suppression. A 2.5 × 2.5 × 2.5 cm^3 MRS voxel was placed in the posterior segment (Couinaud segments 6 or 7) of the right hepatic lobe while avoiding large vessels in the same attempted location for both acquisitions, but without reference to images from the first time point. Imaging parameters for MRS included the following: TR = 3500 ms, 2048 readout points, 1 average, and spectral width (receiver bandwidth) = ±2.5 kHz. To perform T_2 correction in postprocessing, echo times of 10, 20, 30, 40, and 50 ms were acquired (30), within a single 21-s breath hold.

Postprocessing and Image Reconstruction

An investigational, modified IDEAL water–fat estimation reconstruction was used to correct for confounding factors of T_2^* decay, multiple spectral peaks of fat, noise bias, and eddy currents. Reconstructed images were displayed and edited in DICOM format. ROI analysis was performed on the DICOMs on a GE Advantage workstation (GE Healthcare, Waukesha, WI). Researchers commonly assess fat content in the liver using “signal fat-fraction,” which is a useful metric that is independent of B_1 coil sensitivity profiles, providing a normalized measurement of fat concentration. Signal fat-fraction (η) images are generated on a pixel-by-pixel basis using fat images (S_f) and water images (S_w), where:

$$\eta = \frac{S_f}{S_f + S_w} \quad [1]$$

When all confounding factors have been accounted for and/or corrected, the signal fat-fraction is equivalent to the PDFF, which is the ratio of unconfounded signal from all mobile protons of fat, and the sum of the total unconfounded signal from mobile protons in water and fat. For the purposes of this work, we will use the term “fat-fraction” for brevity.

Because estimates of $R_2^*(=1/T_2^*)$ are generated as part of T_2^* correction, as described by Yu et al (23), an R_2^* map is also generated, where the estimated value of R_2^* is displayed on a pixel-by-pixel basis throughout the liver. This T_2^* correction method assumed a that water and fat have the same T_2^* decay in a voxel.

A flip angle of 5° was used to minimize T_1 bias, although simulations have shown that small residual T_1 bias may remain (31). However, methods exist to correct for this bias (13,31), using assumed values of T_1 for fat and water of 343 ms and 586 ms, respectively, as previously reported (32). The amount of T_1 bias was calculated using the TR and assumed values for the T_1 of fat and water, and used to correct the estimated MRI fat-fractions (31). Using simulation results, T_1 bias correction was performed separately from the image reconstruction using measured MRI fat-fractions in Excel.

A single operator at a separate institution blinded to time points and patient information performed the MRS postprocessing using jMRUI (31). A Matlab based program that uses a singular-value decomposition (SVD)-based approach to combine the signals from individual coils was used (33). Spectra were then read into jMRUI and analyzed using the AMARES algorithm. Using prior knowledge, the total fat signal was calculated by summing the signals from peaks located at identical locations as the multi-peak fat spectrum used for MRI (30).

The water and fat signals were corrected for T_2 relaxation by nonlinear fitting of the peaks areas from the different TEs. A priori knowledge of the fat spectrum was then used to correct for the fat peaks near or under the water peak to give a T_2-corrected MRS fat-fraction (34,35).

Statistical Analysis

Two independent readers recorded fat-fraction and R_2^* from the reconstructed fat fraction and R_2^* maps, respectively, measured in nine regions of interest (ROIs) corresponding to each of the nine Couinaud segments. Because the vascular anatomy was difficult to visualize on fat-fraction images when the fat-fraction was low, ROIs were selected on water images and copied to the identical location of the corresponding fat-fraction images and R_2^* maps. In this way, any bias caused by immediate feedback from seeing the ROI value on the monitor during ROI positioning was avoided. Care was taken to avoid large blood vessels and any liver lesions for ROI selection. ROIs from individual segments were matched to the anatomy between Time 1 and Time 2 to the best of each reader's ability. ROIs were identical in size between individual segments for the two time points.

In addition, an ROI was placed at the same location in the MRI fat-fraction image as the MRS voxel using the location of the MRS voxel, which was recorded in the spectroscopy file. Three ROIs of 2.5×2.5 cm^2 were recorded to more closely reflect the three-dimensional shape of the MRS voxel. One ROI was measured at the recorded location of the MRS voxel, which was at the center of the MRS voxel, and an identical ROI was copied to the slices immediately superior and inferior to the center slice. The measurements from the three ROIs were averaged to report a MRI fat-fraction at the location of the MRS voxel. Because both readers would record an identical ROI using the recorded voxel location, an MRI ROI measurement at the location of the MRS voxel was performed for Reader 1 only.

Subsequent analysis was performed on the nine individual fat-fraction ROIs recorded in the Couinaud segments, one fat-fraction ROI at the location of the MRS voxel, and an average fat-fraction of the ROIs recorded in the Couinaud segments; a weighted average by size of ROI was calculated such that an average fat-fraction across the entire liver was reported. ROIs differed in size for each segment, although average ROI size was 152 pixels (range, 55–751 pixels, maximum and minimum located in segments 1 and 8, respectively).

Precision of MRI fat-fraction measurements was assessed through Bland-Altman analysis between time points for both readers using individual ROIs and average fat-fraction across the liver. Bland-Altman plots were also generated for MRS data between time points of processed spectra and for the MRI fat-fractions acquired at the location of the MRS voxel. Precision of MRI R_2^* measurements was also assessed through Bland-Altman analysis between time points for both readers using individual ROIs across the liver only. Corresponding 95% confidence intervals and concordance correlation coefficients between each compared data were also estimated (36).

Accuracy was assessed through linear regression and calculation of the concordance correlation coefficient between the MRI fat-fraction measurement co-registered with the T_2-corrected MRS fat-fraction measurement pooled for Time 1 and Time 2, as recorded by Reader 1. Two-sided t-tests were performed to determine whether statistically significant differences exist between estimated slope values and 1.0, and obtained intercept values and 0.0 ($\alpha = 0.05$).

Sensitivity and specificity for the diagnosis of steatosis, not separated by reader or time point, of the MRI fat-fraction measured at the location of the MRS voxel were calculated

using MRS-determined 5.56% as the diagnostic threshold of steatosis (15,37). Sensitivity and specificity, not separated by time point, of the average fat-fraction across the liver were also calculated. The area under the receiver operating characteristic curve (AROC) was calculated for MRI fat-fractions at the location of the MRS voxel and average MRI fat-fractions using MRS as a reference.

Regression was performed between average MRI fat-fraction and BMI for patients who had recorded height and weight information (n = 30), to determine whether a relationship existed between hepatic fat-fraction and BMI. Next, using a cutoff of a BMI of 25 kg/m^2, patients were divided into two groups (BMI above 25 kg/m^2 and BMI below 25 kg/m^2). Average MRI fat-fractions from each group were plotted against BMI. A modified Levene's test was performed on the average MRI fat-fractions of each BMI group. The modification of this test was based on deviations from the median, rather than the mean, such that the modified Levene's test performed an analysis of variance test based on absolute deviations from the group median. Lastly, a linear regression between average R_2^* values and average MRI fat-fractions for both readers was performed to determine if a relationship existed between hepatic fat-fraction and R_2^* values.

Bland-Altman analysis, and linear regression were performed using Excel (v10 SP3, Microsoft, Redmond, WA). Calculation of concordance correlation coefficients was performed using R v2.8.1 and the Levene's test and AROC calculations were performed using R v 2.10.0 (R Development Core Team, 2009) (38).

Results

Figure 1 displays representative MRI fat-fraction images and corresponding MRS spectra at Time 1 and Time 2 of three patients in this study. Patient 1 (top row) was referred for evaluation of a focal nodular hyperplasia (not shown on this slice), but no known liver disease otherwise, and displays an example of abnormally elevated fat-fraction. Average MRI fat-fraction among both readers and time points was 33.4 ± 0.7% and was 34.2 ± 0.6% for MRS averaged over the two measurements. Patient 2 (middle row) has a history of hepatitis C and cirrhosis. This patient had an elevated MRI fat-fraction of 6.5 ± 0.1% averaged across readers and time points, and an MRS fat-fraction of 7.3 ± 0.1% averaged across time points. Similarly, Patient 3 (bottom row) displays a normal fat-fraction (15,37). Patient 3 had a history of renal cell carcinoma, and underwent an MRI to rule out liver metastases, although he/she has no history of diffuse liver disease. Average MRI fat-fraction among both readers and time points was 1.2 ± 0.2%, and average MRS fat-fraction was 1.3 ± 0.2% across time points. These examples indicate excellent agreement between the two techniques, time points, and readers.

The average fat-fraction among males was 5.72 ± 6.03% (range, 0.00–22.03%) and among females was 5.71 ± 9.00% (range, 0.54–36.45%). A two-tailed t-test showed no statistically significant differences in fat-fractions between genders (P = 0.99).

Precision

Figure 2 shows a Bland-Altman plot between MRI fat-fraction measured at Time 1 and 2 for the nine measured ROIs in the Couinaud segments for both readers (369 points per reader). These results demonstrate both close agreement between readers and time points, and that fat-fraction measured with MRI provides very precise fat-fractions. The limits of agreement encompass 95% of the data, are in units of absolute percent, and effectively constitute the 95% confidence interval (CI). Results from Reader 1 were slightly more precise than Reader 2, where the limits of agreement were [−2.54%, 2.44%] for Reader 1 and [−2.76%, 2.64%]

for Reader 2. When the data for Time 1 and Time 2 were not separated by reader (i.e., pooled), the limits of agreement are [−2.66%, 2.64%].

Figure 3 displays a Bland-Altman plot of the average MRI fat-fraction across the liver for all patients between Time 1 and Time 2 (41 points per reader). As averaging reduces variability, the limits of agreement were [−0.66%, 0.64%] for Reader 1 and [−0.93%, 0.93%] for Reader 2. When average MRI fat-fraction across the liver were pooled the limits of agreement were [−0.81%, 0.79%] between Time 1 and 2.

Figure 4 displays a Bland-Altman plot between fat-fractions from Time 1 and 2 for the MRS data (41 points); the limits of agreement were [−2.69%, 2.87%].

Figure 5 displays a Bland-Altman plot between R_2^* measurements from Time 1 and 2 for both readers (369 points per reader). The limits of agreement of R_2^* measurements were [−15.19 s^{-1}, 13.84 s^{-1}] for Reader 1 and [−19.67 s^{-1}, 18.42 s^{-1}] for Reader 2. When not separated by reader, the limits of agreement for R_2^* measurements were [−17.39 s^{-1}, 16.23 s^{-1}]. The average R_2^* value for both readers and time points was 31.4 ± 10.2 s^{-1} (range, 9.3–182.8 s^{-1}), and the average T_2^* value was 35.0 ± 12.0 ms (range, 5.5–107.6 ms).

As steatosis is known to be heterogeneous across the liver (39), Figure 6 plots the standard deviation over the liver against the average fat-fraction over the liver to assess the variability across segments as a function of the average fat-fraction. Data are shown for Reader 1 at Time 1 and Time 2, where both the standard deviation and average are expressed in fat-fraction percent (%). No patient had a fat-fraction below 0% over the liver, although ROIs from individual segments can be below 0% due to noise. Lower variance is seen at low fat-fractions, but the variance is relatively independent from fat-fraction and plateaus at higher fat-fractions. No strong correlation between the standard deviation and average of the fat-fraction is seen since obtained slope, intercept, and r^2 is 0.07 ± 0.01, 3.02 ± 0.09, and 0.35, respectively.

Precision can be evaluated by the calculation of concordance correlation coefficients (r_c), where values of 1.0 correspond to perfect agreement. Correlation between Time 1 and Time 2 for the MRS fat-fractions is 0.98. Correlation between Time 1 and Time 2 for Reader 1 (Reader 2) using the fat-fraction ROIs measured in the Couinaud segments was 0.98 (0.97), and between readers for Time 1 (Time 2) was 0.97 (0.98). Similarly, correlation between Time 1 and Time 2 for Reader 1 (Reader 2) using the average fat-fraction across the liver was 0.99 (0.99), and between readers for Time 1 (Time 2) was 0.99 (0.99). Similarly, correlation between R_2^* measurements between Time 1 and Time 2 for Reader 1 (Reader 2) was 0.71 (0.59), and between readers for Time 1 (Time 2) was 0.71 (0.48). These results indicate that the readers are in high agreement with each other, and that both MRS and MRI show high agreement for repeated measures. Furthermore, fat-fraction measured with both MRI and MRS are highly precise, and that these results are independent of reader.

Accuracy

MRI provides highly accurate measures of fat-fraction using MRS as a reference standard, as seen by the regression between MRI fat-fraction measured at the MRS voxel location and MRS fat-fraction for Reader 1 in Figure 7. Perfect agreement would have a slope of 1.0 and an intercept of 0.0. Estimated slope, intercept, and r^2 are 1.04 ± 0.02, 0.06 ± 0.21, and 0.96, respectively. The slope and intercept are not significantly different from 1.0 and 0.0, respectively ($P = 0.07$, and $P = 0.8$, respectively). Of note, the intercept indicates high accuracy, particularly at low fat-fractions. For comparison, the estimated slope, intercept, and r^2 for MRI fat-fraction measured at the MRS voxel location *without* T_1 bias correction

versus MRS fat-fraction (not shown, for brevity) are 1.09 ± 0.02, 0.11 ± 0.22, and 0.96, respectively, indicating slight overestimation of the fat-fraction by MRI without correction for residual T_1 bias. Without correction for residual T_1 bias, the slope of 1.09 is significantly different from 1.0 ($P = 0.0006$) although the intercept is not significantly different from 0.0 ($P = 0.6$). The calculated concordance correlation coefficient between MRI fat-fraction at the location of the MRS voxel and MRS fat-fractions was 0.977 for Time 1 and 0.976 for Time 2. Concordance correlation between MRS fat-fraction and average MRI fat-fractions across the liver for Reader 1 at Time 1 (Time 2) was 0.74 (0.64) and for Reader 2 at Time 1 (Time 2) was 0.75 (0.63).

Sensitivity and Specificity

Sensitivity and specificity for diagnosis of steatosis were calculated using MRI fat-fractions colocalized to the MRS voxel. A 5.56% fat-fraction as diagnostic threshold for steatosis, using MRS as the reference standard (37), was used. The fat-fraction measurements at the location of the MRS voxel had a sensitivity and specificity of 91% and 93%, respectively. Using MRS as a reference, AROC for MRI fat-fraction measurements at the location of the MRS voxel was 0.97.

In addition to comparing the sensitivity and specificity of MRI fat-fractions colocalized to the MRS voxel, the sensitivity and specificity of average MRI fat-fractions were compared. As with the previous comparison, a 5.56% fat-fraction as diagnostic threshold for steatosis, using MRS as the reference standard, was used. For the average MRI fat-fractions across the liver, sensitivity and specificity were 100% and 94%, respectively, for both readers. Using MRS as a reference, AROC for average fat-fractions across the liver was 0.97.

Body Mass Index

An exponential relationship is seen between MRI fat-fraction and body mass index (BMI), as shown in Figure 8A MRI fat-fraction is pooled for both readers, and the line of best fit is $y = 0.165e^{0.1089x}$, with an r^2 value of 0.55, indicating good agreement The data are not linear and an exponential relationship empirically fit the data better than other types of curve fitting that were tested.

Using a cutoff of a BMI of 25 kg/m^2, patients were divided into two groups. Average MRI fat-fractions were plotted against these two cutoff groups (above 25 and below 25) in Figure 8B. All patients with a BMI under 25 have average MRI fat-fractions below 5.56% (range, 1.18%–2.25%), or the threshold of a diagnostic indicator of steatosis. Patients with a BMI above 25 display a wider range of fat-fractions (range, 1.04%–33.72%). Using a confidence level of 0.05, results of the modified Levene's test indicated statistically significant differences ($P = 0.0034$) in the median of each BMI patient group.

Relationship Between R_2^* and Fat-Fraction

In addition, no agreement is seen between R_2^* values and average MRI fat-fractions. For both readers and time points, the line of best fit for R_2^* versus average MRI fat-fractions is $y = 0.0336x + 32.206$, with an r^2 value of 0.0011 (plot not shown).

Discussion

In this work, we have evaluated the precision and accuracy of a T_1-independent, T_2^*-corrected chemical shift based water–fat separation method that uses multi-peak spectral modeling of fat and eddy current correction, using MRS as the reference standard. Our results indicate that hepatic fat-fraction measured with MRI is both precise and accurate.

True changes in hepatic fat-fraction exist when longitudinal differences are outside the interval [−2.66%, 2.64%] for side-by-side single ROI measurements, [−0.81%, 0.80%] for a weighted average of nine ROI measurements across the liver, or [−2.69%, 2.87%] for a single MRS measurement. The precision of a single MRS measurement is similar to that of the side-by-side precision, as only one measurement is taken in the liver for each method, and MRS precision is similar to that described by van Werven et al (40). As seen in this study, MRI fat-fractions have similar or better precision than MRS fat-fraction imaging. Furthermore, the precision determined by Bland-Altman analysis is supported by the concordance correlation coefficients, which are all greater than 0.97. For MRS or MRI, these intervals may prove useful for noninvasive longitudinal treatment monitoring of NAFLD to determine whether an observed change is meaningful, and establishment of these intervals to analyze the longitudinal precision of hepatic fat quantification was the primary aim of this work.

In addition, fat-fractions measured with MRI was shown to be as accurate as that measured with MRS. To the best of our knowledge, this is the first study that has performed validation studies of both the precision and accuracy of a quantitative MRI method that corrects for the combination of T_1 bias, noise bias, T_2^* decay, spectral model of fat, and the effects of eddy currents in patients. Furthermore, we successfully reproduced the accuracy results that have been previously reported (25), which was the secondary aim of this work, and these results show that the technique is accurate over a larger patient population.

An advantage to using a whole liver imaging method is that it has the ability to take multiple measurements to improve precision, and an improvement in the precision of fat-fraction imaging is certainly seen when multiple ROIs are recorded across the liver. Taking multiple ROIs may be recommended for future clinical use, as it can more accurately assess the liver in the presence of heterogeneous steatosis and improve precision, although the optimal number and placement of ROIs has yet to be determined. Furthermore, it is well-known that steatosis occurs heterogeneously across the liver (39), and as this technique has been successfully validated, it can be performed to thoroughly analyze fat concentration in segments of the liver.

In this work we have also investigated the ability of MRI to establish a diagnosis of steatosis using MRS as a reference. Sensitivity and specificity of MRI fat-fraction measurements at the location of the MRS voxel were lower than that using average MRI fat-fractions. This improvement in detection of steatosis from using averaged fat-fraction measurements may occur because while the variability of single fat-fraction measurements at low fat-fraction is small, the averaging operation further improves precision of measurements. While variability of fat-fraction can occur across the liver, this variability is probably low at fat-fractions near 5.56%. The reduction in variability achieved through averaging multiple ROIs in different Couinaud segments probably dominates the variability of fat-fraction near the thresh-hold and may explain why sensitivity and specificity of averaged MRI fat-fraction is higher than that from a single ROI colocalized to the MRS voxel.

Furthermore, this work has established the precision of R_2^* measurements in the liver that are provided simultaneously as part of the T_2^* correction for the fat-fraction measurements. For two readers, the limits of agreement are [$-17.39\ s^{-1}$, $16.23\ s^{-1}$]; this range determines the change that must be observed to classify it as a true longitudinal change. Average T_2^* values in this study (35.0 ± 12.0 ms) are consistent with reported values in normal subjects, such as that of Schwenzer et al (28.1 ± 7.1 ms) (41), although a smaller cohort was used for this work and our study examined patients with a variety of liver diseases. Of note, lower correlation and precision was seen between readers and time points for R_2^* measurements,

which is still under investigation. However, differences in R_2^* values did not appear to affect the measured fat-fraction since high correlation and precision are still seen for the fat-fraction results.

A potential limitation of this study was the use of assumed values of T_1 of fat and water for correction of the residual T_1 related bias, beyond that achieved through use of a small flip angle. If actual T_1 values in patients are different than the assumed values, the T_1 bias correction may be incorrect. However, published values of T_1 of fat and water were used in the calculation of the bias (32). Regardless, without any T_1 correction, the correlation between MRI and MRS was excellent, with near perfect statistical agreement. Further optimization between SNR and T_1 bias for SPGR acquisitions is currently being performed, as higher flip angles are preferred to maximize SNR, although they lead to greater overestimation of fat. Another limitation of this study was the lack of biopsy correlation and the use of MRS as the reference standard for determination of accuracy. In addition, no specific group of patients were recruited for this study, rather, we recruited “all-comer” patients undergoing routine abdominal MRI examinations. However, steatosis is a disease feature, not a diagnosis, and is common to many types of liver disease.

In conclusion, proton density fat-fraction, when measured with T_1 independent, T_2^* corrected MRI with multi-peak spectral modeling and eddy current correction is a precise and accurate method to quantify hepatic fat content, when using T_2-corrected MRS as a reference standard. This method provides reliable in vivo fat quantification in patients and is promising as a quantitative biomarker of hepatic steatosis.

Acknowledgments

The authors gratefully acknowledge support from NIH (R01 DK083380, R01 DK088925 and RC1 EB010384), the Coulter Foundation, Bracco Diagnostics, and GE Healthcare.

Contract grant sponsor: NIH; Contract grant numbers: R01 DK083380-01, R01 DK088925-01, RC1 EB010384-01; Contract grant sponsor: Coulter Foundation; University of Wisconsin IEDR.

References

1. Sass DA, Chang P, Chopra KB. Nonalcoholic fatty liver disease: a clinical review. Dig Dis Sci. 2005; 50:171–180. [PubMed: 15712657]
2. Harrison SA, Neuschwander-Tetri BA. Nonalcoholic fatty liver disease and nonalcoholic steatohepatitis. Clin Liver Dis. 2004; 8:861–879. ix. [PubMed: 15464659]
3. Marchesini G, Brizi M, Bianchi G, et al. Nonalcoholic fatty liver disease: a feature of the metabolic syndrome. Diabetes. 2001; 50:1844–1850. [PubMed: 11473047]
4. Marchesini G, Brizi M, Morselli-Labate AM, et al. Association of nonalcoholic fatty liver disease with insulin resistance. Am J Med. 1999; 107:450–455. [PubMed: 10569299]
5. Brunt EM. Nonalcoholic steatohepatitis. Semin Liver Dis. 2004; 24:3–20. [PubMed: 15085483]
6. McCullough AJ. The clinical features, diagnosis and natural history of nonalcoholic fatty liver disease. Clin Liver Dis. 2004; 8:521–533. viii. [PubMed: 15331061]
7. Cuadrado A, Orive A, Garcia-Suarez C, et al. Non-alcoholic steatohepatitis (NASH) and hepatocellular carcinoma. Obesi Surg. 2005; 15:422–426.
8. Smedile A, Bugianesi E. Steatosis and hepatocellular carcinoma risk. Eur Rev Med Pharmacol Sci. 2005; 9:291–293. [PubMed: 16231592]
9. Ratziu V, Charlotte F, Heurtier A, et al. Sampling variability of liver biopsy in nonalcoholic fatty liver disease. Gastroenterology. 2005; 128:1898–1906. [PubMed: 15940625]
10. Thomsen C, Becker U, Winkler K, Christoffersen P, Jensen M, Henriksen O. Quantification of liver fat using magnetic resonance spectroscopy. Magn Reson Imaging. 1994; 12:487–495. [PubMed: 8007779]

11. Wong WF, Northrup SR, Herrick RC, Glombicki AP, Wood RP, Morrisett JD. Quantitation of lipid in biological tissue by chemical shift magnetic resonance imaging. Magn Reson Med. 1994; 32:440–446. [PubMed: 7997107]
12. Bohte AE, van Werven JR, Bipat S, Stoker J. The diagnostic accuracy of US, CT, MRI and (1)H-MRS for the evaluation of hepatic steatosis compared with liver biopsy: a meta-analysis. Eur Radiol. 2011; 21:87–97. [PubMed: 20680289]
13. Bydder M, Yokoo T, Hamilton G, et al. Relaxation effects in the quantification of fat using gradient echo imaging. Magn Reson Imaging. 2008; 26:347–359. [PubMed: 18093781]
14. Reeder SB, Robson PM, Yu H, et al. Quantification of hepatic steatosis with MRI: the effects of accurate fat spectral modeling. J Magn Reson Imaging. 2009; 29:1332–1339. [PubMed: 19472390]
15. Yokoo T, Bydder M, Hamilton G, et al. Nonalcoholic fatty liver disease: diagnostic and fat-grading accuracy of low-flip-angle multiecho gradient-recalled-echo MR imaging at 1.5 T. Radiology. 2009; 251:67–76. [PubMed: 19221054]
16. Hu HH, Kim HW, Nayak KS, Goran MI. Comparison of fat-water MRI and single-voxel MRS in the assessment of hepatic and pancreatic fat fractions in humans. Obesity (Silver Spring). 2009; 18:841–847. [PubMed: 19834463]
17. Hines CD, Yu H, Shimakawa A, et al. Quantification of hepatic steatosis with 3-T MR imaging: validation in ob/ob mice. Radiology. 2010; 254:119–128. [PubMed: 20032146]
18. Sirlin CB, Reeder SB. Magnetic resonance imaging quantification of liver iron. Magn Reson Imaging Clin N Am. 2010; 18:359–381. ix. [PubMed: 21094445]
19. Liu CY, McKenzie CA, Yu H, Brittain JH, Reeder SB. Fat quantification with IDEAL gradient echo imaging: correction of bias from T(1) and noise. Magn Reson Med. 2007; 58:354–364. [PubMed: 17654578]
20. Fishbein MH, Gardner KG, Potter CJ, Schmalbrock P, Smith MA. Introduction of fast MR imaging in the assessment of hepatic steatosis. Magn Reson Imaging. 1997; 15:287–293. [PubMed: 9201675]
21. Hussain HK, Chenevert TL, Londy FJ, et al. Hepatic fat fraction: MR imaging for quantitative measurement and display--early experience. Radiology. 2005; 237:1048–1055. [PubMed: 16237138]
22. Yu H, Shimakawa A, McKenzie CA, Brodsky E, Brittain JH, Reeder SB. Multiecho water-fat separation and simultaneous R2* estimation with multifrequency fat spectrum modeling. Magn Reson Med. 2008; 60:1122–1134. [PubMed: 18956464]
23. Yu H, McKenzie CA, Shimakawa A, et al. Multiecho reconstruction for simultaneous water-fat decomposition and T2* estimation. J Magn Reson Imaging. 2007; 26:1153–1161. [PubMed: 17896369]
24. Yu, H.; Shimakawa, A.; Reeder, SB.; McKenzie, CA.; Brittain, JH. Magnitude fitting following phase sensitive water-fat separation to remove effects of phase errors. Proceedings of the 17th Annual Meeting of ISMRM; Honolulu. 2009. abstract 462
25. Meisamy S, Hines CD, Hamilton G, et al. Quantification of hepatic steatosis using T1 independent, T2* corrected MRI with accurate spectral modeling: a blinded comparison with 1H MR spectroscopoy. Radiology. Epub ahead of print.
26. Hines CD, Yu H, Shimakawa A, et al. T1 independent, T2* corrected MRI with accurate spectral modeling for quantification of fat: validation in a fat-water-SPIO phantom. J Magn Reson Imaging. 2009; 30:1215–1222. [PubMed: 19856457]
27. Reeder SB, McKenzie CA, Pineda AR, et al. Water-fat separation with IDEAL gradient-echo imaging. J Magn Reson Imaging. 2007; 25:644–652. [PubMed: 17326087]
28. Beatty, PJ.; Brau, AC.; Chang, P., et al. A method for autocalibrating 2-D accelerated volumetric parallel imaging with clinically practical reconstruction times. Proceedings of the 15th Annual Meeting of ISMRM; Berlin. 2007. abstract 1749
29. Brau AC, Beatty PJ, Skare S, Bammer R. Comparison of reconstruction accuracy and efficiency among autocalibrating data-driven parallel imaging methods. Magn Reson Med. 2008; 59:382–395. [PubMed: 18228603]

30. Hamilton G, Middleton MS, Bydder M, et al. Effect of PRESS and STEAM sequences on magnetic resonance spectroscopic liver fat quantification. J Magn Reson Imaging. 2009; 30:145–152. [PubMed: 19557733]

31. Hines, CD.; Yokoo, T.; Bydder, M.; Sirlin, CB.; Reeder, SB. Optimization of flip angle to allow tradeoffs in T1 bias and SNR performance for fat quantification. Proceedings of the 18th Annual Meeting of ISMRM; Stockholm. 2010. abstract 2927

32. de Bazelaire CM, Duhamel GD, Rofsky NM, Alsop DC. MR imaging relaxation times of abdominal and pelvic tissues measured in vivo at 3.0 T: preliminary results. Radiology. 2004; 230:652–659. [PubMed: 14990831]

33. Bydder M, Hamilton G, Yokoo T, Sirlin CB. Optimal phased-array combination for spectroscopy. Magn Reson Imaging. 2008; 26:847–850. [PubMed: 18486392]

34. Hamilton G, Yokoo T, Bydder M, et al. In vivo characterization of the liver fat 1H magentic resonance spectrum. NMR Biomed. 2010 in press.

35. Sharma P, Martin DR, Pineda N, et al. Quantitative analysis of T2-correction in single-voxel magnetic resonance spectroscopy of hepatic lipid fraction. J Magn Reson Imaging. 2009; 29:629–635. [PubMed: 19243059]

36. Lin L, Torbeck LD. Coefficient of accuracy and concordance correlation coefficient: new statistics for methods comparison. PDA J Pharm Sci Technol. 1998; 52:55–59. [PubMed: 9610168]

37. Szczepaniak LS, Nurenberg P, Leonard D, et al. Magnetic resonance spectroscopy to measure hepatic triglyceride content: prevalence of hepatic steatosis in the general population. Am J Physiol Endocrinol Metab. 2005; 288:E462–E468. [PubMed: 15339742]

38. R Development Core Team R. A language and environment for statistical computing. Vienna: R Foundation for Statistical Computing; 2009.

39. Hamer OW, Aguirre DA, Casola G, Lavine JE, Woenckhaus M, Sirlin CB. Fatty liver: imaging patterns and pitfalls. Radiographics. 2006; 26:1637–1653. [PubMed: 17102041]

40. van Werven JR, Hoogduin JM, Nederveen AJ, et al. Reproducibility of 3.0 Tesla magnetic resonance spectroscopy for measuring hepatic fat content. J Magn Reson Imaging. 2009; 30:444–448. [PubMed: 19629974]

41. Schwenzer NF, Machann J, Haap MM, et al. T2* relaxometry in liver, pancreas, and spleen in a healthy cohort of one hundred twenty-ine subjects-correlation with age, gender, and serum ferritin. Invest Radiol. 2008; 43:854–860. [PubMed: 19002057]

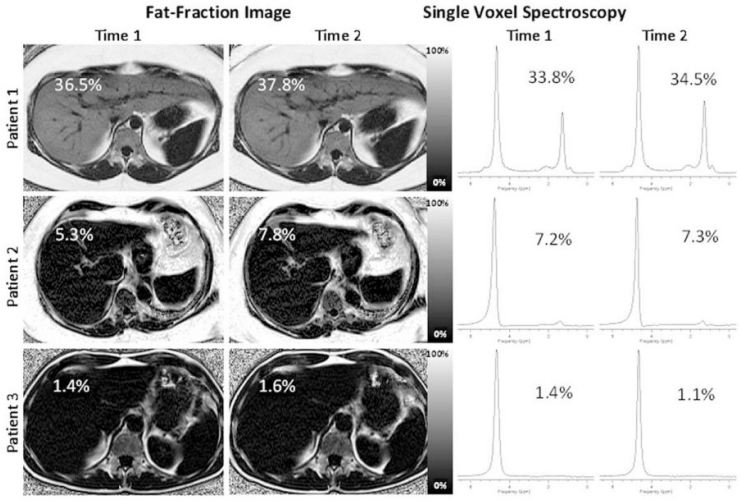

Figure 1.

Representative patient fat-fraction images and MRS spectra at Time 1 and Time 2. Patient 1, Patient 2, and Patient 3 are examples of severely elevated fat-fraction, mildly elevated fat-fraction, and a normal fat-fraction, respectively. The MRI fat-fraction recorded at the location of the MRS voxel is displayed on each fat-fraction image. MRS fat-fractions are as indicated on the spectra. Excellent agreement is seen between time points for individual readers, between different readers, and between techniques.

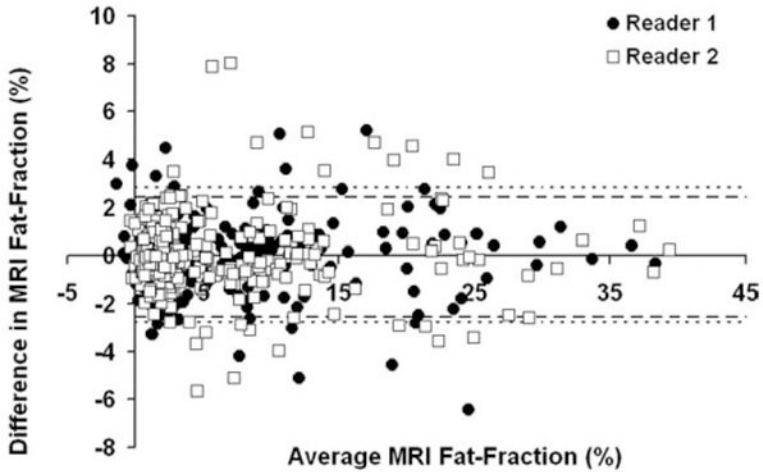

Figure 2.

Bland-Altman plot between Time 1 and Time 2 for the MRI fat-fractions measured in each of the Couinaud segments for all volunteers, indicating high precision. The limits of agreement for Reader 1 (circles) are [−2.54%, 2.44%], denoted as a heavy dashed line. The limits of agreement for Reader 2 (squares) are [−2.76%, 2.83%], denoted as a fine dashed line. If data from both readers is pooled, the limits of agreement are [−2.66%, 2.64%].

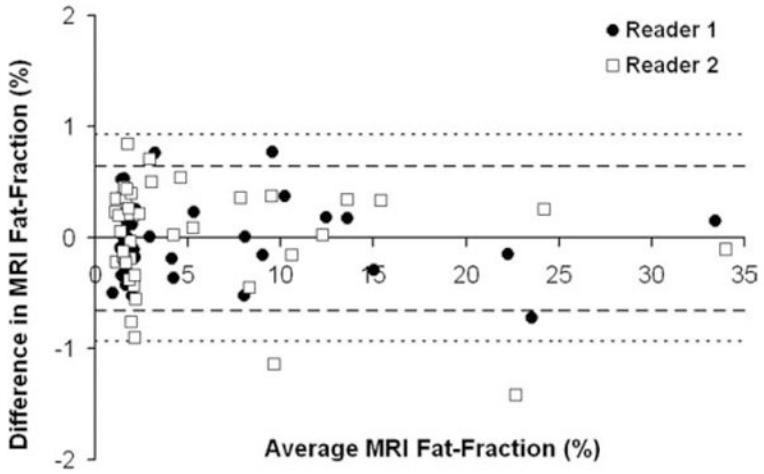

Figure 3.

Bland-Altman plot between Time 1 and Time 2 for average MRI fat-fraction across the liver. The limits of agreement for Reader 1 (circles), denoted as a heavy dashed line, are [−0.66%, 0.64%] and for Reader 2 (squares), denoted as a fine dashed line, are [−0.94%, 0.93%]. If data from both readers is pooled, the limits of agreement are [−0.81%, 0.80%].

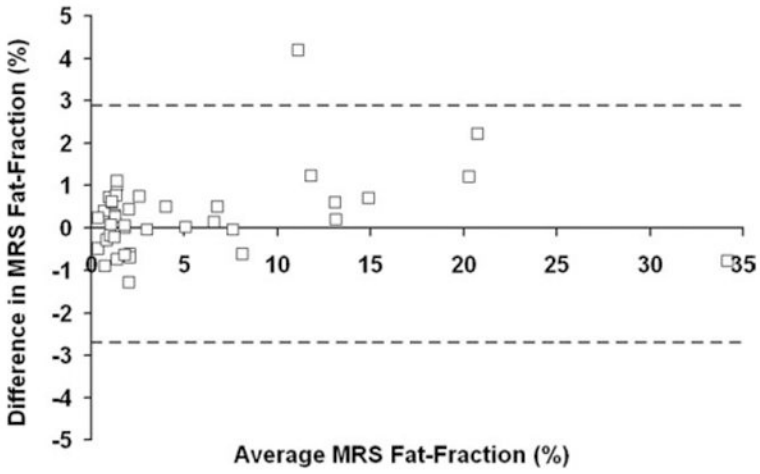

Figure 4.
Bland-Altman plot between Time 1 and Time 2 for MRS fat-fraction. The limits of agreement are [−2.70%, 2.87%].

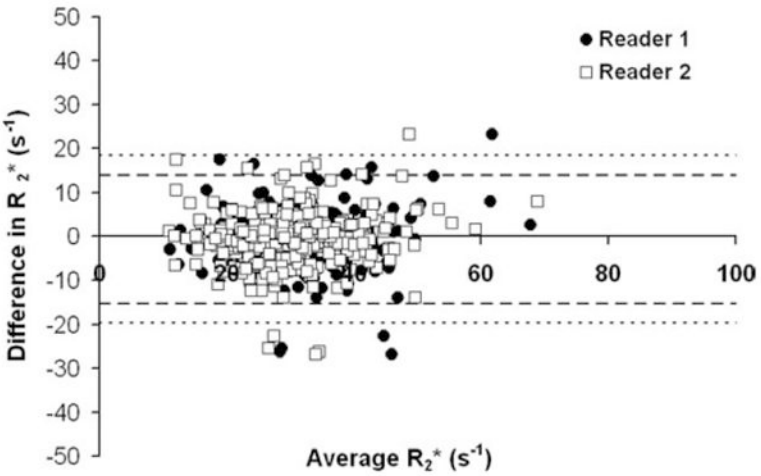

Figure 5.

Bland-Altman plot between Time 1 and Time 2 for R_2^* measurements. The limits of agreement for Reader 1 (circles), denoted as a heavy dashed line, are [−15.19 s^{-1}, 13.84 s^{-1}], and for Reader 2 (squares), denoted as a fine dashed line, are [−19.67 s^{-1}, 18.42 s^{-1}]. If data from both readers is pooled, the limits of agreement are [−17.39 s^{-1}, 16.23 s^{-1}].

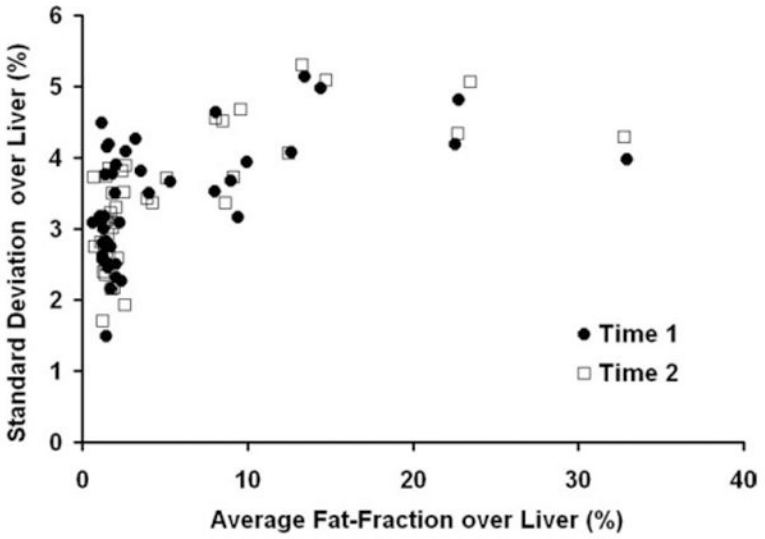

Figure 6.
Standard deviation over the liver versus average fat-fraction over the liver for Reader 1 at Time 1 and Time 2. Both axes are expressed in fat-fraction percent (%). A lower variance is seen in most patients that have low fat-fractions. In general, however, the variance of measurements was relatively independent as the variance plateaus at approximately 5% for a wide range of fat-fractions.

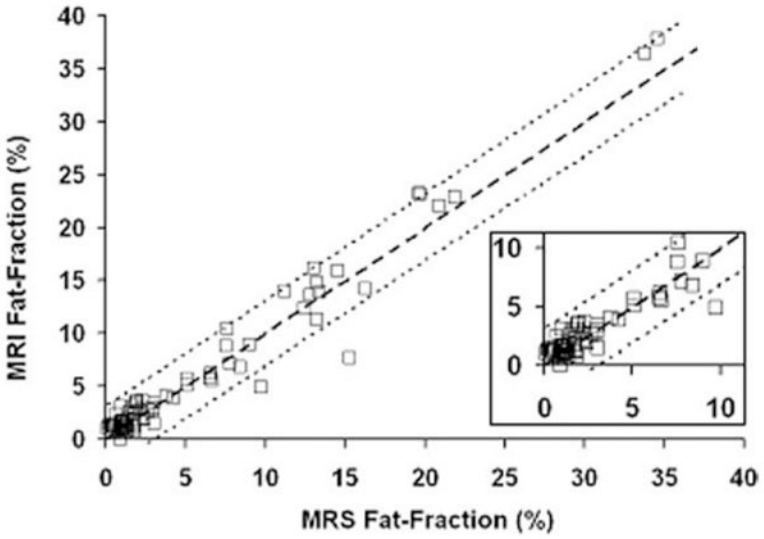

Figure 7.

Linear regression of MRI fat-fraction measured in the location of the MRS voxel and MRS fat-fraction indicates high accuracy. Estimated slope, intercept, and r^2 value are 1.04 ± 0.02, 0.06 ± 0.21, and 0.96, respectively. The slope and intercept are not significantly different from 1.0 and 0.0, respectively. An inset zoom of the 0–10% region is shown in the lower right hand corner. Heavy dashed line is unity, and 95% confidence interval of the slope is as fine dashed lines.

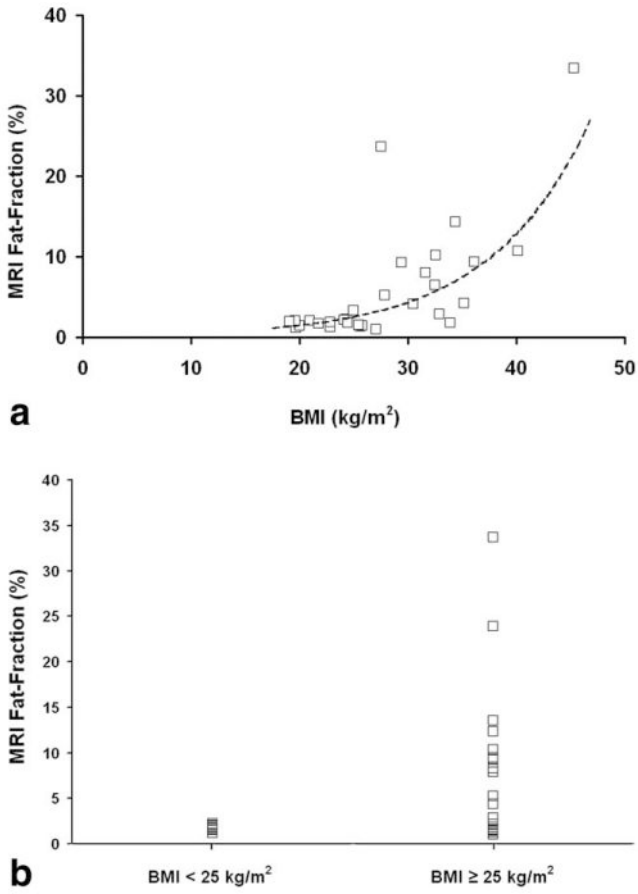

Figure 8.

a: Regression of average MRI fat-fraction and BMI displays an exponential relationship for pooled readers. Line of best fit is $y = 0.165e^{0.1089x}$ and r^2 is 0.55. **b:** Comparison of average MRI fat-fraction versus patients with a BMI above and below 25 kg/m^2. All patients with a BMI below 25 kg/m^2 have fat-fractions that are considered normal or healthy, although a wider range of fat-fractions is seen in patients with a BMI above 25 kg/m^2.